Mineralogical Magazine (2025), **89**, 830–842
doi:10.1180/mgm.2025.10108

Article

Jagoite revisited: crystal structure, mineral composition and paragenesis

Dan Holtstam[1], Fernando Cámara[2], Andreas Karlsson[1] and Thomas Zack[3]

[1]Department of Geosciences, Swedish Museum of Natural History, Stockholm, Sweden; [2]Dipartimento di Scienze della Terra 'A. Desio', Via Luigi Mangiagalli, Università degli Studi di Milano, Milano, Italy; and [3]Department of Earth Sciences, University of Gothenburg, Göteborg, Sweden

Abstract

The rare Pb silicate jagoite, known only from the Långban and Pajsberg Mn–Fe oxide deposits in Värmland, Sweden, is associated with a more diverse mineral assemblage than originally described: alamosite, barysilite, hyttsjöite, margarosanite, melanotekite, nasonite and yangite and other, not fully characterised Pb silicates. Primary melanotekite and barysilite, formed as skarn (together with hematite, quartz, clinopyroxene and andradite) during regional metamorphism, are prone to alteration, with Cl^{-}, SiO_2, Ca^{2+} and H_2O acting as modifying agents. In the process, newly formed Pb silicates exhibit increasing Si content, reflecting a higher degree of SiO_4 polymerisation at high pH and decreasing temperatures.

A refinement of the crystal structure of jagoite from X-ray diffraction data, to $R1 = 1.2\%$ [space group $P\bar{6}2c$, $a = 8.53926(5)$ Å and $c = 33.3399(2)$ Å], confirms previous work, and provides significantly improved structural parameters. New data were also obtained with Mössbauer spectroscopy, laser-Raman micro-spectroscopy, electron-microprobe and laser-ablation inductively coupled plasma mass spectrometry analyses. The results indicate that jagoite accommodates minor elements, notably Al at an octahedrally coordinated Fe-dominated site and Mn^{3+}, Zn and Mg at four-coordinated mixed Fe–Si sites, and small amounts of Ca+Na replacing Pb. Jagoite is also enriched in Be, Sb, Bi and Br, but those elements have a limited role in its crystal chemistry. Mössbauer measurements show that Fe^{3+} is distributed over three different crystallographic sites, two 4-coordinated and one 6-coordinated, and that jagoite remains paramagnetic down to 77 K. The ideal chemical formula for jagoite should be written $Pb_{11}Fe_5Si_{12}O_{41}Cl_3$ for $Z = 2$.

Keywords: jagoite; Pb silicate; crystal structure; Mössbauer spectroscopy; skarn; Långban-type deposit; Värmland; Sweden

(Received 28 March 2025; revised 5 June 2025; accepted 5 June 2025; Accepted Manuscript published online: 15 July 2025)

Introduction

Lead silicates form a diverse category of compounds, occurring in both natural mineral assemblages (skarns and hydrothermal veins) and in anthropogenic formations (e.g. ceramics and metallurgical slags). The diversity is underpinned by the behaviour of the Pb^{2+} ion, with a stereo-active lone pair of electrons, and its influence on the structural arrangement of the tetrahedral SiO_4 units (e.g. Siidra *et al.*, 2014). The inclusion of other metals in the crystal structures further expands the possibilities for diversification. As an environmental pollutant, Pb can be immobilised in silicate phases (Li *et al.*, 2012), but the element may also be released during hydrothermal or supergene alteration of those (e.g. Davis *et al.*, 1993). This is a motivation to study these compounds further.

About 50 different Pb silicates are known as minerals, most of them restricted to a few prolific ore localities, like the Långban Fe–Mn mine and its satellite deposits in the Filipstad district, Värmland, Sweden (Moore, 1970; Holtstam and Langhof, 1999), Franklin-Sterling Hill, New Jersey (Dunn, 1985) and the Kombat mine, Namibia (Dunn, 1991). We have reinvestigated jagoite, a very rare mineral with the formula $Pb_{18}Fe^{3+}{}_4[Si_4(Si,Fe^{3+})_6][Pb_4Si_{16}(Si,Fe)_4]O_{82}Cl_6$. It was described briefly by Blix *et al.* (1957) from Långban and the crystal structure was later solved by Mellini and Merlino (1981). For this study, we used the type material, and additional samples not studied in detail before, from Långban and the Pajsberg Mn–Fe deposit (both Filipstad, Värmland).

Geological setting

The carbonate-hosted Långban-type Fe–Mn–(Ba–Pb–As–Sb) deposits are associated with Palaeoproterozoic (Orosirian period), mainly rhyolitic volcanic and volcanoclastic country rocks in the Bergslagen ore province (formally: the Bergslagen lithotectonic unit; Stephens and Jansson, 2020) of south-central

Corresponding author: Dan Holtstam; Email: dan.holtstam@nrm.se
Guest Editor: Robert F. Martin
This paper is part of a collection in tribute to the work of Edward Grew at 80
Cite this article: Holtstam D., Cámara F., Karlsson A. and Zack T. (2025) Jagoite revisited: crystal structure, mineral composition and paragenesis. *Mineralogical Magazine* **89**, 830–842. https://doi.org/10.1180/mgm.2025.10108

© The Author(s), 2025. Published by Cambridge University Press on behalf of The Mineralogical Society of the United Kingdom and Ireland. This is an Open Access article, distributed under the terms of the Creative Commons Attribution licence (http://creativecommons.org/licenses/by/4.0), which permits unrestricted re-use, distribution and reproduction, provided the original article is properly cited.

Table 1. Electron-microprobe analyses of type jagoite, GEO-NRM #19410178

Component	(wt.%)									Mean	2σ
SiO_2	20.25	20.68	20.21	20.37	20.46	20.54	20.68	20.13	20.00	20.37	0.45
Al_2O_3	0.17	0.21	0.16	0.11	0.09	0.17	0.06	0.14	0.15	0.14	0.09
Mn_2O_3	1.03	1.02	1.03	0.98	0.91	0.96	1.09	0.93	1.10	1.01	0.11
Fe_2O_3	6.80	6.70	6.77	7.25	7.02	7.35	6.63	6.66	6.62	6.86	0.52
CaO	0.27	0.32	0.30	0.36	0.28	0.29	0.37	0.25	0.35	0.31	0.08
ZnO	0.36	0.33	0.43	0.32	0.35	0.35	0.44	0.63	0.40	0.40	0.18
PbO	66.31	65.59	66.11	65.93	66.86	66.50	65.03	65.48	66.39	66.02	1.08
Cl	3.20	3.07	3.27	3.13	3.23	3.07	3.23	3.14	3.05	3.15	0.15
Sum	98.39	97.92	98.27	98.45	99.20	99.23	97.53	97.36	98.06	98.26	
$O \equiv Cl$										−0.71	
Total										97.55	

Sweden. This unique kind of mineralisation, known for its exceptional wealth of rare minerals, is attributed to a combination of exhalative–sedimentary, high-grade metamorphic and hydrothermal processes (Boström *et al.*, 1979; Holtstam and Mansfeld, 2001). Metal-enriched sediments were deposited at ~1.9 Ga from exhalative-volcanogenic solutions in a shallow-submarine, oxidising environment. During subsequent tectonic and metamorphic events, culminating during the Svecofennian orogeny (~1.85 Ga), the primary ores recrystallised and intense skarn formation occurred. (Note that the term 'skarn' here is used in its original, non-genetic sense referring to silicate mineral assemblages associated with ore.) Peak conditions in the Långban area are estimated at 600 ± 50°C and 0.3–0.4 GPa (Christy and Gatedal, 2005; Skelton *et al.*, 2018). Later brittle deformation and hydrothermal activity, possibly related to the Sveconorwegian (1.2–0.9 Ga) orogeny, have played a crucial role in the remobilisation of key elements and further evolution of the deposits and led to the formation of various late-stage minerals (mostly in fissures at temperatures < 200°C and low lithostatic pressure; Jonsson and Broman, 2002), contributing significantly to the species diversity here.

Methods

Selected representative samples from the collections of the Swedish Museum of Natural History, Department of Geosciences, have been investigated. For single-crystal work and spectroscopy, crystals from the type specimen #19410178 were used. All samples were examined under a FEI Quanta 650 field-emission-gun scanning electron microscope (SEM), fitted with a back-scattered electron (BSE) detector and an 80 mm^2 X-Max^N Oxford Instruments energy-dispersion (EDS) micro-analyser, on polished sections in carbon-coated epoxy mounts. Powder X-ray diffraction (PXRD) using a PANalytical X'Pert PRO diffractometer (Cu$K\alpha$ radiation) was used for complementary mineral identification.

Electron-microprobe analyses (EMPA) of type jagoite (Table 1) were collected with an AZtecWave wavelength-dispersion (WDS) system attached to the SEM as above, at 20 kV and 14 nA, with a working distance of 10 mm. Mineral reference materials were used as follows: jadeite (Na$K\alpha$), almandine (Al, Si, Ca$K\alpha$), rhodonite (Mn$K\alpha$), hematite (Fe$K\alpha$), willemite (Zn$K\alpha$), crocoite (Pb$L\alpha$) and tugtupite (Cl$K\alpha$). Sodium, Mg and K were close to or below the detection limit with this method. Low analytical results were observed occasionally and may be related to inadequate conduction on detached mineral grains embedded in epoxy.

In situ chemical analyses by laser-ablation inductively coupled plasma mass spectrometry analyses (LA-ICP-MS) on jagoite (Table 2) were carried out with a New Wave Research 213 nm laser coupled to an Agilent 8800 MS/MS at the University of Gothenburg. The data were retrieved from two analytical sessions, one with a 70 μm circular spot and a laser repetition rate of 10 Hz, corresponding to a fluency of 5 J/cm^2. For the second analytical session a laser spot of 50 μm was used, with all other settings kept the same. We used NIST SRM610 as the primary standard for minor and trace element quantification, with exceptions for Cl (sodalite, ILM127; Zahoransky *et al.*, 2016) and Br (doped basaltic glass, GSE-1g, Marks *et al.*, 2017; Caulfield *et al.*, 2020). Silica was used as an internal standard, which in turn was derived from electron-microprobe data. The accuracy and precision of the concentrations of minor and trace elements were evaluated with data on BCR2-g and GSE1-g. The elements S, Te, I and Th were sought but found to be close to or below the level of detection. Values obtained for Fe_2O_3 and CaO (wt.%), respectively, are 6.86±0.52, 0.31±0.08 (WDS) vs. 6.30±0.27, 0.30±0.07 (LA-ICP-MS) for the type specimen, confirming a good agreement between the methods for metals.

Single-crystal X-ray diffraction data were collected from a thin crystal fragment (dimensions 0.189 × 0.085 × 0.030 mm) and with a sensitive detector, HyPix, mounted on a XtaLAB Synergy by Rigaku, using Mo$K\alpha$ radiation. A dataset of 46 runs of 0.5° wide images were collected at 15 and 40 seconds for a total of 6604 images to ensure full coverage of the reciprocal space and correct absorption correction.

The crystal structure of jagoite was refined by using *Olex 2* v. 1.3 (Dolomanov *et al.*, 2009) and *SHELXL* 2018/3 (Sheldrick, 2015) starting from the atom coordinates of Mellini and Merlino (1981) using neutral scattering curves and refining Fe versus Al in the Fe octahedron, Si versus Fe in the *Si*1 and *Si*2 tetrahedra, Si in the *Si*3, *Si*4 and *Si*5 tetrahedra, Pb at the *Pb*1, *Pb*2 and *Pb*3 sites, Cl at the *Cl*1 site and oxygen at the nine anion sites in the asymmetric unit. The experimental and crystal data are summarised in Table 3. Atomic coordinates, displacement parameters and calculated bond-valences are given in Table 4. Bond distances are reported in Table 5. The crystallographic information file of this study has been deposited with the journal and is available as Supplementary material (see below).

Transmission ^{57}Fe Mössbauer spectra were obtained from a 30 mg jagoite powder absorber mixed with 100 mg acrylic resin and pressed into a circular tablet. To exclude contamination of the powder with alteration products and foreign inclusions, crystal fragments were hand-picked under the binocular microscope.

https://doi.org/10.1180/mgm.2025.10108 Published online by Cambridge University Press

Table 2. Element concentrations in jagoite from LA-ICP-MS analyses (μg/g)

Sample:	19440122 (n = 15)			19410178 (n = 21)				19440122 (n = 15)			19410178 (n = 21)		
	Mean	Min	Max	Mean	Min	Max		Mean	Min	Max	Mean	Min	Max
Li	13	6.5	20	39	27	64	Se	0.47	0.23	1.0	0.47	0.22	0.90
Be	36	29	44	122	100	150	Br	556	508	598	525	452	560
B	1.2	0.95	2.1	0.96	0.64	1.3	Rb	0.11	0.02	0.45	0.05	0.02	0.08
Na	851	680	1048	807	644	1251	Sr	21	19	22	16	9.1	30
Mg	1086	420	2332	918	650	2062	Y	0.02	0.01	0.13	0.02	0.01	0.07
Al	756	383	1197	714	323	2361	Zr	5.0	2.0	13	2.9	0.82	11
P	4.0	1.3	8.4	4.7	1.8	11	Nb	1.8	1.1	2.4	5.7	2.2	10
Cl	27054	26346	27549	27441	26901	28000	Mo	0.17	0.08	0.28	0.16	0.07	0.24
K	62	44	136	37	28	62	Cd	0.38	0.27	0.67	0.26	0.15	0.45
Ca	2002	1833	2559	2176	1962	3156	In	0.05	0.02	0.09	0.05	0.01	0.08
Ti	148	66	314	13	5.2	28	Sn	1.7	0.35	4.8	1.4	0.11	4.5
V	0.93	0.50	1.5	0.51	0.44	0.60	Sb	708	365	1063	1682	1281	2710
Cr	0.53	0.38	1.1	0.54	0.18	3.1	Cs	0.02	0.01	0.06	0.01	0.01	0.05
Mn	6164	5763	6716	6491	5549	7145	Ba	7.7	6.3	10	269	232	289
Fe	44016	43115	45990	44715	42958	46758	Ce	0.18	0.11	0.35	0.77	0.30	1.2
Co	0.32	0.27	0.42	0.63	0.47	0.75	Hf	0.08	0.01	0.24	0.04	0.00	0.11
Ni	0.16	0.07	0.50	0.11	0.07	0.30	Ta	0.09	0.05	0.14	0.08	0.04	0.20
Cu	0.05	0.02	0.11	0.04	0.01	0.09	W	0.41	0.20	0.59	0.56	0.10	1.61
Zn	6278	5545	7758	4642	3212	5529	Tl	0.01	0.01	0.03	0.01	0.01	0.02
Ga	2.1	1.7	2.6	30	26	34	Bi	27	21	37	13	9.1	19
Ge	3.7	2.2	4.5	2.9	1.9	4.5	U	0.19	0.06	0.73	1.5	0.35	2.5
As	1.1	0.45	2.1	0.81	0.48	1.4							

n = number of analyses.

Table 3. Crystal data and structure refinement for jagoite, sample GEO-NRM #19410178

Temperature/K	293(2)
Radiation	Mo$K\alpha$ (λ = 0.71073)
Crystal system	hexagonal
Space group	$P\bar{6}2c$
a/Å	8.53926(5)
c/Å	33.3399(2)
Volume/Å^3	2105.40(3)
Z	2
ρ_{calc}/mg·mm^{-3}	5.723
μ/mm^{-1}	43.153
$F_{(000)}$	3008.0
Crystal size/mm^3	0.189 × 0.085 × 0.030
2θ range for data collection	4.888 to 59.998°
Index ranges	$-12 \le h \le 12$
	$-12 \le k \le 12$
	$-46 \le l \le 46$
Reflections collected	68990
Independent reflections	2090[R_{int} = 0.0437]
Data/restraints/parameters	2090/0/123
Goodness-of-fit on F^2	1.276
Final R indexes [$I \ge 2\sigma$ (I)]	R_1 = 0.0123, wR_2 = 0.0287
Final R indexes [all data]	R_1 = 0.0123, wR_2 = 0.0287
Largest diff. peak/hole/e Å^{-3}	1.29/−0.67
Flack parameter	0.004(2)

Weight = $1/[\sigma^2(F_o^2) + (0.0481 \times P)^2 + 34.76 \times P]$ where $P = (\text{Max}(F_o^2, 0) + 2 \times F_c^2)/3$.

A test run with PXRD showed only jagoite in the purified sample, with refined unit-cell parameters a = 8.5530(6) and c = 33.376(5) Å. For the experiments, ^{57}Co γ-radiation (Rh matrix source, nominally 1.8 GBq) and a constant-acceleration spectrometer (WissEl) were used. Two-mirror image spectra (± 4.28 mm/s) were collected at 54.7° geometry to avoid preferred-orientation effects, at 298 K and 77 K (with a liquid-nitrogen cryostat) during 15 and 5 days, respectively, over 1024 channels. The raw data were calibrated against a 25 μm iron foil. The *MossA* software (Prescher *et al.*, 2012) was employed for spectrum analysis, under the assumption of Lorentzian line shapes and a 'thin' absorber.

Raman spectra were obtained from randomly orientated polished grains using a LabRAM HR 800 micro-spectrometer. The analysis employed a 514 nm Ar-ion laser source with a power output of ∼1 mW, a Peltier-cooled (−70°C) 1024 × 256 pixel CCD detector (Synapse), and an Olympus M Plan N 100×/0.9 NA objective, providing a laser spot size of ∼3 μm. A 600 grooves/cm grating was used, achieving a resolution of about 1 cm^{-1}. Peak positions were calibrated against the Raman band at 789 cm^{-1} of a silicon carbide crystal measured on {0001}. Data acquisition and instrument control were managed with *LabSpec 5* software, covering a spectral range of 100–4000 cm^{-1}, with 30 second exposure times repeated over five cycles.

Results

Mineral assemblages

The description by Blix *et al.* (1957) of the mineral association is skeletal; the mineral was found in hematite ore from the Canberra stope (at 220 m depth; Magnusson, 1930) of the Långban mine in the 1940s, together with melanotekite, quartz and an unidentified mineral.

From the present study, it is clear that the mineral assemblage is a highly heterogeneous skarn, in contact with dolomitic marble, with ubiquitous andradite, pyroxene (diopside–aegirine), hematite and quartz, plus three or more of the lead silicates alamosite, barysilite, hyttsjöite, jagoite, margarosanite, melanotekite, nasonite and yangite, in each specimen (Figs 1–4). Most of these minerals approach their nominal chemical compositions (see Table 6).

https://doi.org/10.1180/mgm.2025.10108 Published online by Cambridge University Press

Table 4. Fractional atomic coordinates and equivalent isotropic displacement parameters (Å^2) for jagoite. U_{eq} is defined as ⅓ of the trace of the orthogonalised U_{ij} tensor. Bond valence sums (BVS) are in valence units (vu)

Atom	Occupancy	*x*	*y*	*z*	*U*(eq)	BVS*
Pb1	0.975(6)	⅓	⅔	0.33066(2)	0.01702(11)	1.82
Pb2	0.950(4)	0.36759(3)	0.41121(3)	0.42424(2)	0.01715(6)	1.96
Pb3	0.911(5)	−0.11098(5)	0.27817(5)	¼	0.02738(12)	1.99
Fe	0.978(16)	0	0	0.43057(3)	0.0145(4)	2.97
Al	0.022(16)					
Si1	0.709(12)	0.27530(15)	0	0	0.0121(4)	3.73
Fe1	0.291(12)					
Si2	0.703(14)	0	0	0.30313(5)	0.0163(5)	3.63
Fe2	0.296(14)					
Si3	0.942(15)	⅔	⅓	0.49635(7)	0.0126(7)	3.87
Si4	0.959(12)	⅔	⅓	0.33925(6)	0.0110(7)	4.09
Si5		0.29013(17)	0.02261(17)	0.36261(4)	0.0150(3)	3.99
Cl1		0.3333(3)	0.4191(3)	¼	0.0387(8)	1.00
O1		0.2211(5)	0.1135(5)	0.39483(10)	0.0188(7)	1.96
O2		0.1026(5)	0.2259(5)	0.46305(11)	0.0213(7)	1.96
O3		⅔	⅓	0.54481(18)	0.0199(12)	1.92
O4		0.1646(7)	0.4778(6)	0.52085(13)	0.0318(10)	1.92
O5		0.1749(4)	0.4336(5)	0.37601(11)	0.0188(7)	2.08
O6		0.9850(7)	0.1900(7)	0.31852(13)	0.0375(12)	2.14
O7		⅔	⅓	0.29115(19)	0.0272(14)	1.91
O8		0.8558(6)	0.3664(6)	0.35745(15)	0.0310(10)	2.08
O9		0	0	¾	0.033(2)	2.15

*Bond valence parameters for cation–oxygen bonds taken from Gagné and Hawthorne (2015) and Brese and O'Keeffe (1991) for cation–chlorine bonds.

Table 5. Bond lengths (Å) and geometrical parameters for jagoite

Pb1–O5^{i}	2.321(4)	Pb2–O1	2.410(4)	Pb3–Cl^{xi}	2.873(2)	Fe–O1^{iv}	2.023(3)		
Pb1–O5	2.321(4)	Pb2–O2	2.391(4)	Pb3–Cl^{xiv}	2.899(2)	Fe–O1^{vii}	2.023(3)		
Pb1–O5^{ii}	2.321(4)	Pb2–O3^{iii}	2.559(2)	Pb3–Cl^{iii}	3.358(3)	Fe–O1	2.023(3)		
Pb1–Cl^{vii}	3.421(2)	Pb2–O4^{iii}	3.016(7)	Pb3–O6^{v}	2.659(5)	Fe–O2^{vii}	1.993(4)		
Pb1–Cl	3.421(2)	Pb2–O5^{iv}	2.376(4)	Pb3–O6^{vi}	2.659(5)	Fe–O2	1.993(4)		
Pb1–Cl^{xiv}	3.421(2)	Pb2–O5^{vii}	2.937(5)	Pb3–O7^{vi}	2.570(3)	Fe–O2^{iv}	1.993(4)		
<Pb1–Φ>	2.871	Pb2–O8^{vii}	3.008(5)	Pb3–O7^{v}	2.570(3)	<Fe–O>	2.008		
V (Å^3)	26.62	<Pb2–O>	2.671	Pb3–O9	2.659(5)	*V* (Å^3)	10.78		
d.i.*	0.1916	*V* (Å^3)	27.71	<Pb3–Φ>	2.819	d.i.	0.0076		
		d.i.	0.1014	*V* (Å^3)	38.12				
				d.i.	0.0725				
Si1–O2^{viii}	1.683(4)	Si2–O6^{x}	1.767(6)	Si3–O3	1.616(6)	Si4–O7	1.604(7)	Si5–O1	1.601(4)
Si1–O2^{9}	1.683(4)	Si2–O6^{xi}	1.767(6)	Si3–O4^{xii}	1.638(4)	Si4–O8^{x}	1.612(4)	Si5–O5^{vii}	1.632(4)
Si1–O4^{8}	1.737(5)	Si2–O6^{vi}	1.767(6)	Si3–O4^{xiii}	1.638(4)	Si4–O8	1.612(4)	Si5–O6^{x}	1.627(4)
Si1–O4^{9}	1.737(5)	Si2–O9^{iii}	1.7715(17)	Si3–O4^{iii}	1.638(5)	Si4–O8^{xiv}	1.612(4)	Si5–O8^{x}	1.643(5)
<Si1–O>	1.710	<Si2–O>	1.768	<Si3–O>	1.633	<Si4–O>	1.610	<Si5–O>	1.626
V (Å^3)	2.55	*V* (Å^3)	2.83	*V* (Å^3)	2.23	*V* (Å^3)	2.14	*V* (Å^3)	2.19
d.i.	0.0159	d.i.	0.0011	d.i.	0.0051	d.i.	0.0021	d.i.	0.0077

Notes: Symmetry codes: (i) +*y*–*x*, 1–*x*, +*z*; (ii) 1–*y*, 1+*x*–*y*, +*z*; (iii) +*y*, +*x*, 1–*z*; (iv) –*y*, +*x*–*y*, +*z*; (v) –1+*x*, +*y*, ½–*z*; (vi) –1+*x*, +*y*, +*z*; (vii) +*y*–*x*, –*x*, +*z*; (viii) +*y*–*x*, –*x*, ½–*z*; (ix) +*y*, +*x*, –½+*z*; (x) 1+*y*–*x*, 1–*x*, +*z*; (xi) –*y*, –1+*x*–*y*, +*z*; (xii) 1–*x*, –*x*+*y*, 1–*z*; (xiii) 1–*y*+*x*, 1–*y*, 1–*z*; (xiv) 1–*y*, +*x*–*y*, +*z*; *distortion index (Baur, 1974).

Jagoite occurs in aggregates of greenish yellow subhedral crystals of a micaceous nature with a perfect {0001} cleavage, in portions of the skarn rich in melanotekite. It is often concentrated in strings that cross-cut the rock matrix but partly follow grain boundaries of pre-existing minerals. Jagoite is in most specimens partly surrounded by fine-grained alteration products, whitish and turbid under the binocular microscope, on fringes and along cleavage planes. In a single specimen (#19610234), a new Pb silicate mineral with an ideal formula $Pb_8Al_3Si_8O_{27}Cl_3$ and similar in physical appearance to jagoite (but colourless), occurs as subhedral grains up to 300 μm in width. These occur in close association with melanotekite and jagoite; the full description of the new mineral, friisite (IMA2024-047; Holtstam *et al.*, 2024), is in progress.

Långban is the second recorded locality of yangite (sample #19410179, Fig. 2a), which was previously only known from its type specimen (Kombat, Namibia; Downs *et al.*, 2016). It occurs as elongated, colourless to slightly wine-yellow crystals in aggregates up to 1 mm. The refined triclinic unit-cell parameters of yangite (based on PXRD data) from Långban are $a = 9.597(2)$ Å, $b = 7.281(2)$ Å, $c = 7.968(2)$ Å, $\alpha = 106.03(1)°$, $\beta = 118.14(1)°$, $\gamma = 109.85(1)°$ and $V = 392.7(1)$ Å^3, in good agreement with original data (Downs *et al.*, 2016). A mineral similar in composition to

https://doi.org/10.1180/mgm.2025.10108 Published online by Cambridge University Press

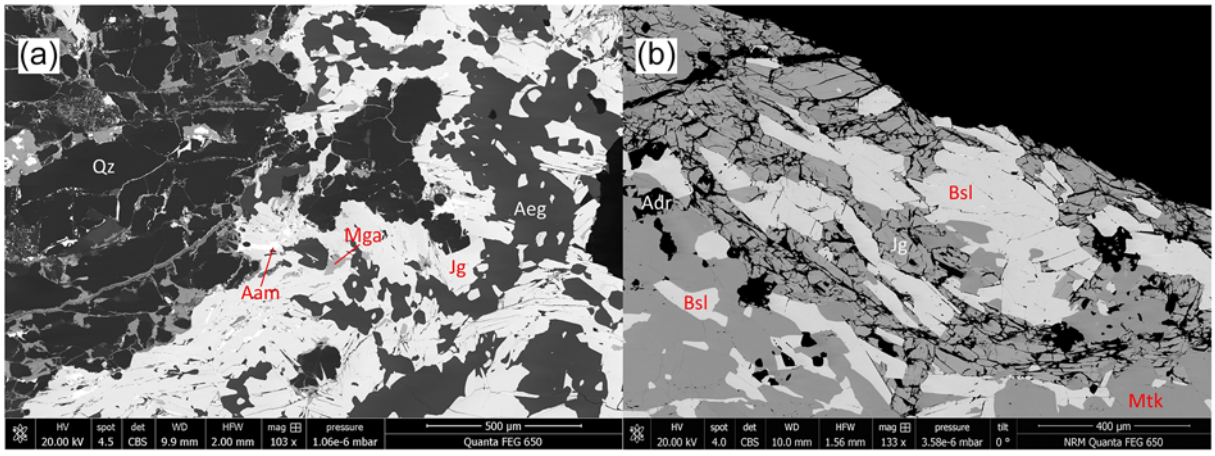


Figure 1. BSE images of polished sections, samples GEO-NRM #19440118 (a) and #g19348 (b). Mineral symbols from Table 6. Adr = andradite; Aeg = aegirine.

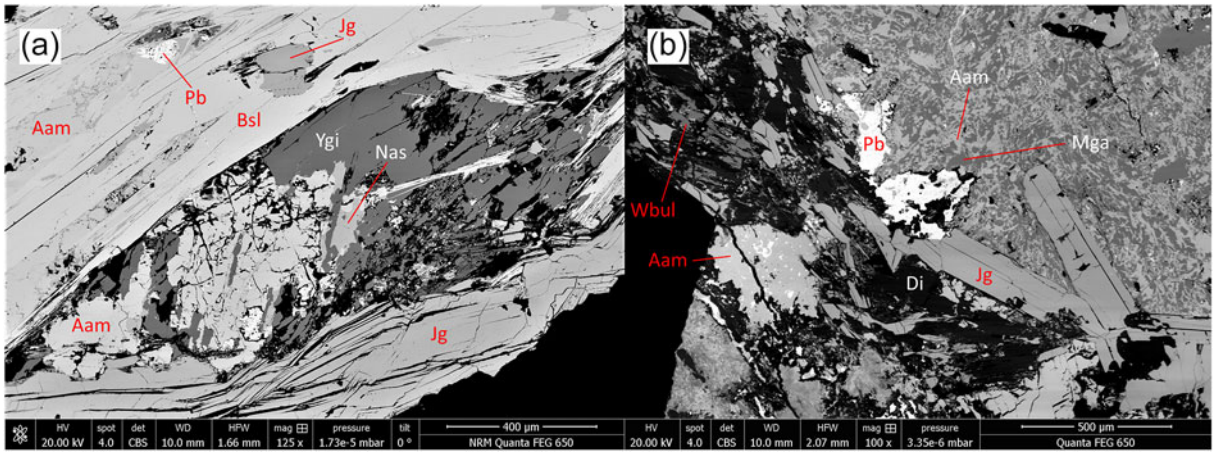


Figure 2. BSE images of polished sections, samples GEO-NRM #19410179 (a) and #19610234 (b). Mineral symbols from Table 6. Di = diopside; Pb = native lead.

wickenburgite ($Pb_3CaAl_2Si_{10}O_{27}{\cdot}4H_2O$, Williams, 1968; possibly a Mn analogue) is found as thin flaky crystals associated with jagoite and alamosite (Fig. 2b).

Margarosanite commonly occurs as a single phase in the alteration zones surrounding jagoite (Fig. 3a), but in some cases also in a eutectoid texture, as intergrowths with alamosite (Fig. 2b), possibly representing remnants of another altered lead silicate. An unknown Pb–Ca–Cl–O–H silicate (described in more detail below) formed during jagoite alteration, has also been observed in several samples (Fig. 3b).

Other minerals occurring in minor or trace amounts in the sample population are: baryte, calcite, native lead, fluorapophyllite-(K), talc, 'serpentine', albite, orlymanite (?) fluorapatite and phosphohedyphane. Minor amounts of additional late-stage alteration phases occur in some specimens, usually comprising very fine-grained material that contains Ca, Mg, Mn, Si ± Al, Pb, Fe and H_2O, but so far are not possible to characterise properly.

On the label of specimen #g19348, it is written 'Pajsberg', which probably means the Stora Pajsberg mine (59°47.04′N; 14°19.03′E), belonging to the Pajsberg Fe–Mn ore field (Lee, 1958; Holtstam *et al.*, 2019). The sample comprises a dense skarn assemblage with diopside, andradite, melanotekite, barysilite, jagoite and minor calcite. In contrast to the Långban specimens, no alteration of jagoite was observed in this case (Fig. 1b).

Table 6. Lead silicates found in the present study (L = Långban, P = Pajsberg)

Mineral	Deposit	Formula	Cations/Si
Alamosite (Aam)	L	$PbSiO_3$	1
Barysilite (Bsl)	L, P	$Pb_8Mn[Si_2O_7]_3$	1.5
Hyttsjöite (Hyj)	L	$Pb_{18}Ba_2Ca_5Mn_2Fe_2Si_{30}O_{90}Cl{\cdot}6H_2O$	0.97
Jagoite (Jg)	L, P	$Pb_{11}Fe_5Si_{12}O_{41}Cl_3$	1.33
Friisite (Fii)	L	$Pb_8Al_3Si_8O_{27}Cl_3$	1.38
Margarosanite (Mga)	L	$PbCa_2Si_3O_9$	1
Melanotekite (Mtk)	L, P	$Pb_2Fe_2[Si_2O_7]O_2$	2
Nasonite (Nas)	L	$Pb_6Ca_4[Si_2O_7]_3Cl_2$	1.67
Unknown (Ukn)	L	$Pb_2Ca_3Si_5Cl_2O_{13}(OH)_2{\cdot}2H_2O$ (?)	1
'Wickenburgite-like' (Wbul)	L	$Pb_3(Mn,Ca)Al_2Si_{10}O_{27}{\cdot}4H_2O$ (?)	0.6
Yangite (Ygi)	L	$PbMnSi_3O_8{\cdot}H_2O$	0.67

Notes: Mineral symbols are after Warr (2021).

The unknown Pb–Ca–Cl silicate

As mentioned, an unknown mineral substance is observed as an abundant alteration product of jagoite in some samples. It has so far resisted our attempts to determine its crystal structure, using both X-ray and electron diffraction methods, despite the fact that is has a

https://doi.org/10.1180/mgm.2025.10108 Published online by Cambridge University Press

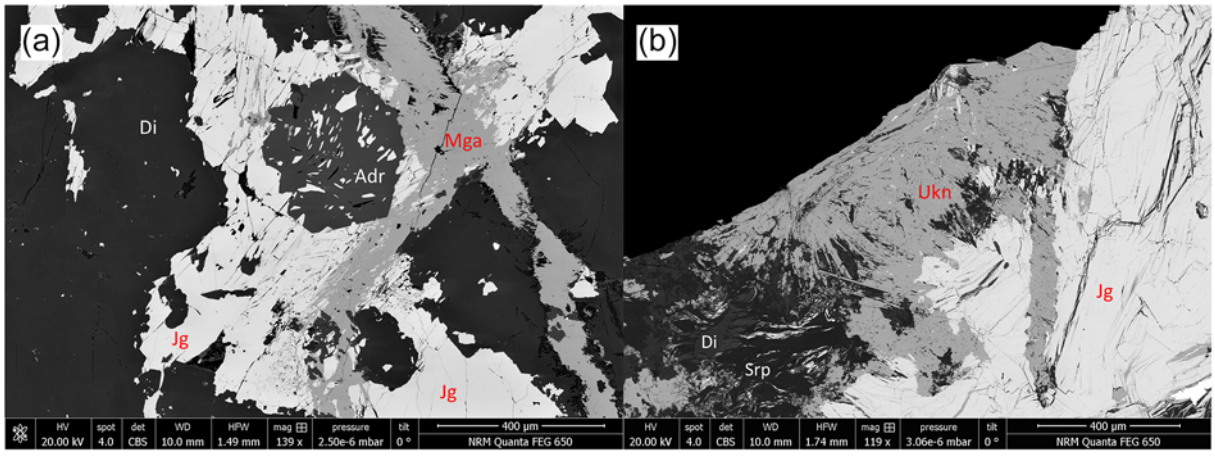


Figure 3. BSE images of polished sections, samples GEO-NRM #19440121 (a) and #19440122 (b) Mineral symbols from Table 6. Adr = andradite; Di = diopside; Srp = 'serpentine'.

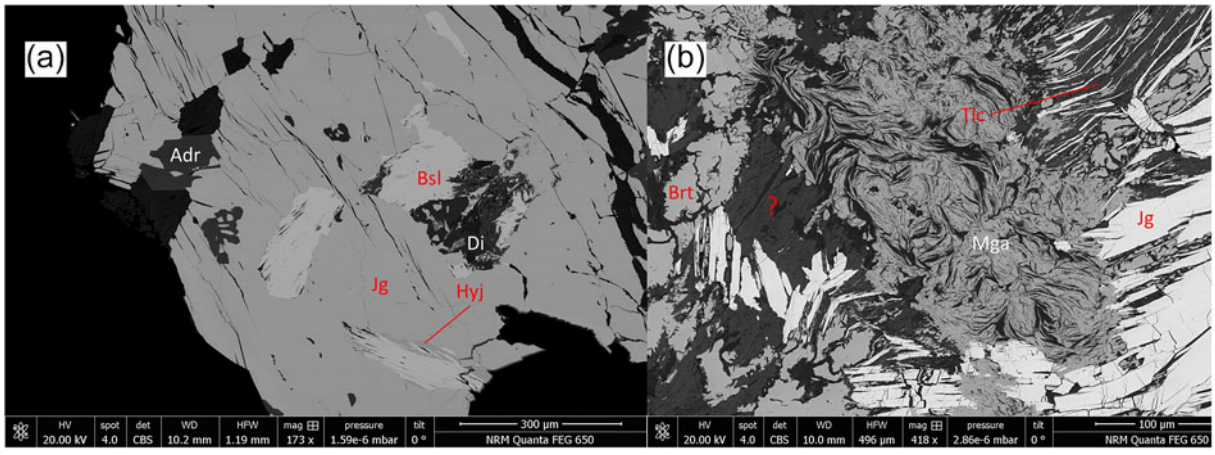


Figure 4. BSE images of polished sections, samples GEO-NRM #19410178 (a) and #19440122 (b). Mineral symbols from Table 6. Adr = andradite; Brt = baryte; Di = diopside; Tlc = talc. The question mark represents an unknown phase with composition close to orlymanite.

unique and reproducible powder X-ray diffraction pattern (Fig. 5). A brief description, which may facilitate recognition of the phase and possibly lead to a full description in the future, is included here. It appears in aggregates with a felt-like, fine-grained texture. The colour is greyish white to beige. The mineral shows a distinct bright yellow fluorescence colour under SW UV light; associated margarosanite and calcite are light blue and orange, respectively, under the same conditions.

The formula can at this point only be approximately determined, to circa $Pb_2Ca_3Si_5Cl_2O_{13}(OH)_2{\cdot}nH_2O$. The composition is based on EDS point analyses, giving SiO_2 28.0, MnO 2.3, CaO 14.8, PbO 44.4, Cl 6.7 (wt.%), and infrared (IR) spectroscopy. The presence of H_2O and OH^- is indicated in the IR spectrum (Fig. 6) from the combination mode at circa 5200 cm^{-1} and the narrow band at 3550 cm^{-1} related to O–H stretching vibrations, respectively. Laser-Raman spectra exhibit a very broad signal centred at ~3600 cm^{-1} (possibly related to fluorescence) but also distinct bands at 1088, 987, 713, 283 and 154 cm^{-1} (Fig. 7).

Physical properties of jagoite

Micro-indentation hardness measurements on randomly orientated grains, obtained by means of a Shimadzu type-M tester for a 15 s indentation time, gave $VHN_{100} = 495$ (=4.85 GPa) based on eleven measurements in a total range of 388–558. The shape of indentations is straight to slightly concave, accompanied by star radial fractures (in the terminology of Jambor and Vaughan, 1990). The microhardness obtained corresponds to a value intermediate to 4 and 5 on the Mohs scale (Broz *et al.*, 2006), which is significantly higher than $H = 3$ reported by Blix *et al.* (1957). The calculated density, 5.73(1) g·cm^{-3}, based on single-crystal unit-cell data and an empirical formula of the type specimen (see below), is also higher than the measured value given by Blix *et al.* (1957), 5.43 g·cm^{-3}.

Crystal structure of jagoite

Refinement of the crystal parameters from single-crystal X-ray diffraction data of the jagoite type specimen [$R_1 = 1.2\%$ for 2089 reflections with $F_o > 4\sigma(F_o)$] gave $a = 8.53926(5)$, $c = 33.3399(2)$ Å with $Z = 12$ and systematic absences compatible with a $P\bar{6}2c$ unit cell, in good agreement with previous results. The structure model by Mellini and Merlino (1981) is corroborated, but our data are a high-resolution dataset obtained from a thin plate. This allows for adequate absorption correction, anisotropic atomic displacement factors and thus a considerable improvement in the accuracy of bond distances and bond angles.

https://doi.org/10.1180/mgm.2025.10108 Published online by Cambridge University Press

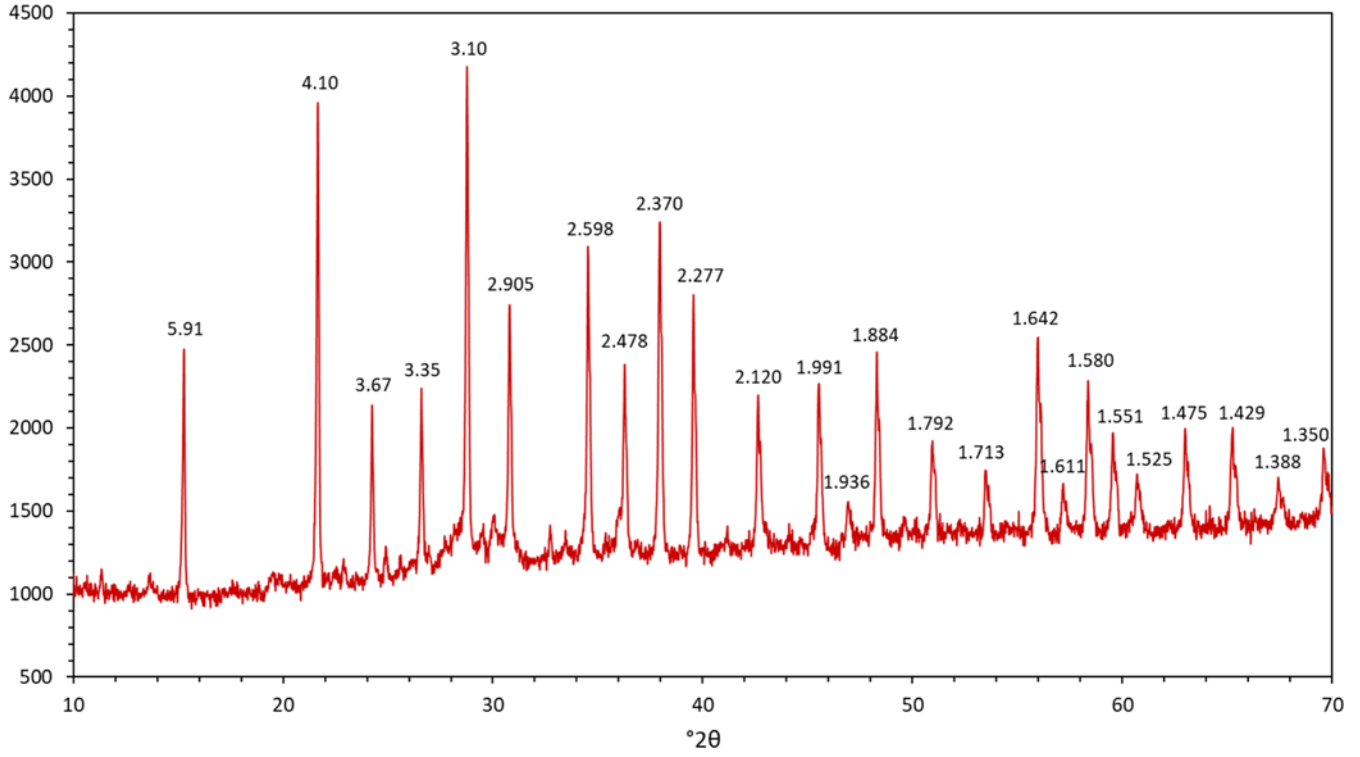


Figure 5. Powder-X-ray diffraction profile of the unknown Pb–Ca–Cl-silicate, sample GEO-NRM #19440122 with *d* values (in Å) of the Bragg peaks indicated. Cu*K*α-radiation data.

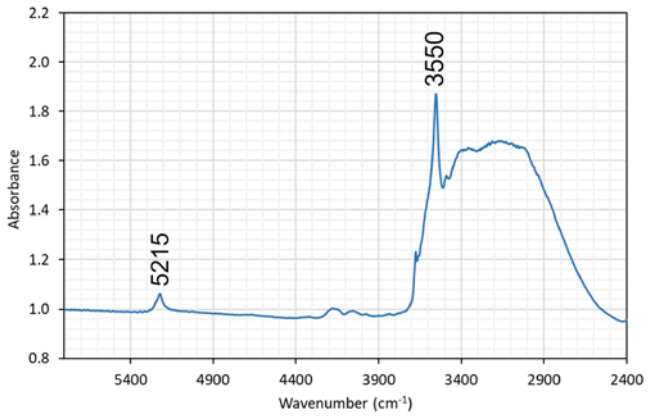


Figure 6. Unpolarised IR spectrum of the unknown Pb–Ca–Cl-silicate obtained on an ~100 μm thick aggregate. Sample GEO-NRM #19884399.

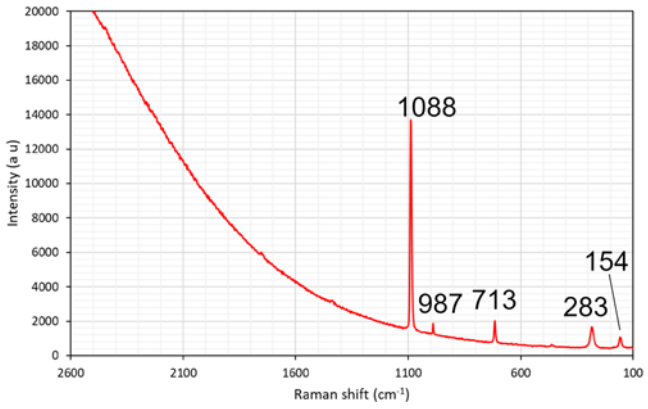


Figure 7. Laser-Raman spectrum of the unknown Pb–Ca–Cl silicate obtained with a 514 nm laser. Sample GEO-NRM #19440122.

Jagoite has a single and a double layer of SiO_4 tetrahedra (Fig. 8), like reyerite $[(Na,K)_2Ca_{14}[Al_2Si_{22}O_{58}](OH)_8(H_2O)_6]$ (Merlino, 1988) and minehillite $[K_2Ca_{28}Al_4[Zn_5\square Si_{40}O_{112}](OH)_{16}]$ (Dai *et al.*, 1995). The single-layer sheet (Fig. 9) is based on the $(12^2)_3(12^3)_2$ net (Hawthorne *et al.*, 2019) that also occurs in zeophyllite (Merlino, 1972) and asbecasite (Sacerdoti *et al.*, 1993). In jagoite, the single layer is linked on both sides to a (FeO_6–PbO_7)-layer. The FeO_6 octahedra occur at the origin in the single layer. The double layer (Fig. 8, left side) hosts Pb (=*Pb*3) and Cl atoms that conform to a $Pb\Phi_8$ layer (Φ = O, Cl) of edge-sharing distorted hexahedra. The Pb1 atom is 6-coordinated (3 × O, 3 × Cl), and *Pb*2 is 7-coordinated (7 × O). Jagoite is also related to wickenburgite $[Pb_3CaAl_2Si_{10}O_{27}{\cdot}4H_2O]$, as in its double layer, one of 12 [(Al, Si)O_4] tetrahedra is replaced by a $[O_3Ca(H_2O)_3]$ octahedron (Hesse *et al.*, 2003).

Two out of five of the tetrahedra in jagoite, *Si*1 and *Si*2, have mixed Si:Fe occupancies. Tetrahedron *Si*2 is the one connecting the two layers of tetrahedra of the double layer. Tetrahedron *Si*1 alternates with Si3 (occupied by only Si) in the single layer, with each *Si*3 surrounded by 3 *Si*1 tetrahedra. Each Si1O_4 tetrahedron is vertex-sharing with two FeO_6 octahedra.

Mineral compositions

The original publication by Blix *et al.* (1957) showed (in wt.%) SiO_2 22.35, BeO 0.12, Al_2O_3 0.50, Fe_2O_3 7.00 TiO_2 0.10, MgO 0.60, MnO

https://doi.org/10.1180/mgm.2025.10108 Published online by Cambridge University Press

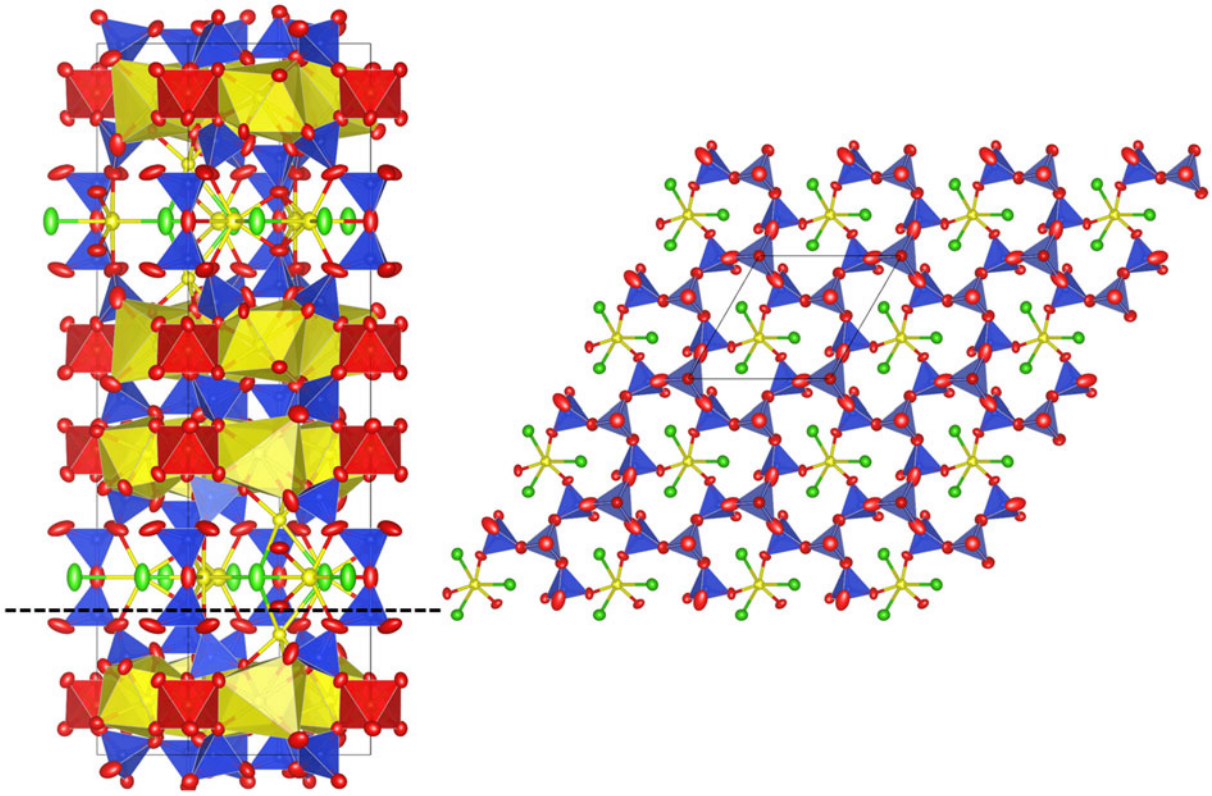


Figure 8. The jagoite crystal structure seen along [010] (left) and [001] at z = 0.20 (right). Symbols: Si tetrahedra = blue. Fe octahedra = red. Pb atoms and polyhedra = yellow. Cl atoms = green. Oxygen atoms = red ellipsoids. Crystal-structure drawings made by *VESTA 3* (Momma and Izumi, 2011).

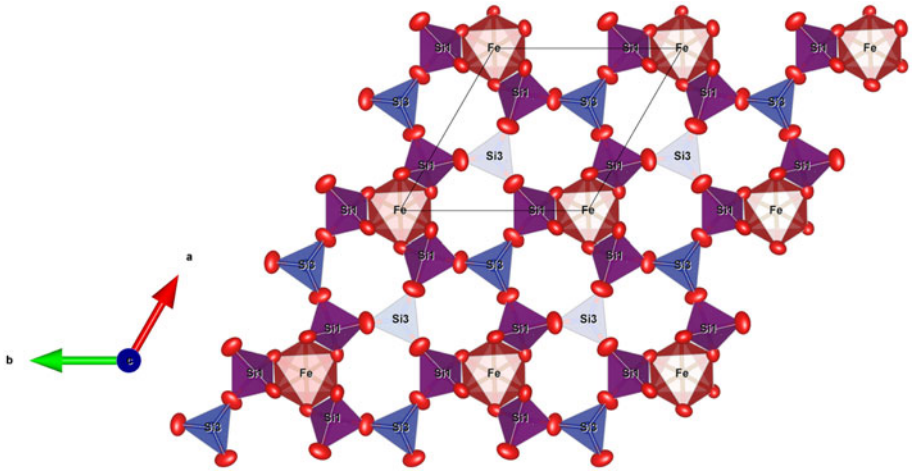


Figure 9. The jagoite crystal structure at $z \approx 0$ seen along [001]. The Si1 tetrahedra with purple colour have a mixed Fe^{3+} + Si occupancy.

0.88, CaO 0.65, PbO 64.26, Na_2O 0.61, K_2O 0.37, Cl 3.25, H_2O 0.36, O ≡ Cl –0.73, total 100.32, from a wet-chemical analysis. Grew *et al.* (1996) reported a single electron-microprobe analysis (WDS) of jagoite from Långban with (in wt.%) SiO_2 22.11, Fe_2O_3 6.43, MnO 0.94, CaO 0.40, PbO 68.00, Cl 3.22, i.e. with similar values as presented here for the type specimen (Table 1).

The LA-ICP-MS data on two samples (Table 2) show that jagoite is poor in most trace elements. Compared to the continental-crust average, however, Be, Sb and Bi are abundant. The enrichment of these elements is characteristic of Långban-type deposits (Holtstam and Mansfeld, 2001; Hålenius *et al.*, 2013). A few elements show larger variations in the two samples analysed, Al (383–2361 ppm), Mg (420–2332 ppm), Ti (5–314 ppm), Ba (6–289 ppm) and Ga (2–34 ppm). The mineral is poor in most first-row transition metals, except Fe, Mn and Zn. In addition to Ca and Na, jagoite is not particularly enriched in large-ion alkali or alkaline earth metals (K, Rb, Cs, Sr and Ba) that could substitute for Pb^{2+} in the crystal structure. Rare earth elements, as indicated by very low concentrations of Y and Ce, are not abundant either. The halogen content is relatively constant; sample 19440122 contains 2.63–2.75 wt.% Cl and 534–596 ppm Br, and the jagoite holotype specimen 19410178 yields similar results,

https://doi.org/10.1180/mgm.2025.10108 Published online by Cambridge University Press

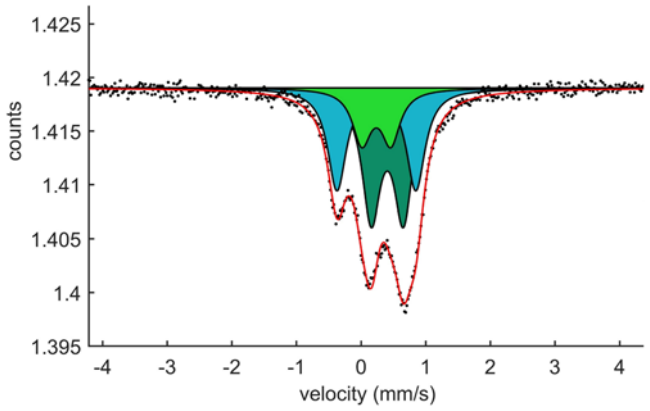


Figure 10. ^{57}Fe Mössbauer spectrum of jagoite at room temperature. Counts given on the *y* axis are ×10^7. Sample GEO-NRM #19410178.

2.69–2.80 wt.% Cl and 447–560 ppm Br. Notably, Cl concentrations obtained by LA-ICP-MS are lower than those obtained by EMPA, but used for the formula calculation because they are considered more reliable (a slight destruction of the surface of the tugtupite reference was noted during the analytical session at the EMPA).

From the compositional information presented here, some shortcomings of the original wet-chemical data of the type material become clear. In particular, concentrations of BeO, MgO, Na_2O, K_2O and H_2O as determined by Blix *et al.* (1957) were too high and should not affect the present empirical formula to the extent that has been suggested before (Mellini and Merlino, 1981). For instance, the results of the present work show the absence of hydrogen (see Raman spectroscopy results) and therefore, OH groups have not been considered a defining element of the ideal formula.

From the combined electron-microprobe and LA-ICP-MS data, the following empirical formula based on 28 cations is obtained:

$$Pb_{10.94}Na_{0.13}Ca_{0.21}Fe^{3+}_{3.18}Sb_{0.05}Zn_{0.18}Mn^{3+}_{0.48}Al_{0.10}Mg_{0.14}Si_{12.54}Be_{0.05}O_{41.12}Cl_{2.86}Br_{0.02.}$$

Mineral spectroscopy

In the Mössbauer spectrum (Fig. 10) obtained at ambient temperature, the best fit ($\chi^2 = 1.1$ in the last cycle of the fitting procedure) with physically reasonable parameters is obtained with a three-doublet model. The hyperfine parameters determined are given in Table 7. Centroid shifts are consistent with Fe atoms being present only in the trivalent state (high spin), and distributed over both 6-coordinated and 4-coordinated sites. The higher quadrupole-splitting value associated with one of the $^{[4]}$Fe doublets is related to the higher degree of distortion of the corresponding coordination polyhedron, thus probably $Si1O_4$ (distortion index 0.0159; Table 5). The Mössbauer pattern obtained at 77 K is very similar to the room-temperature spectrum (except for the expected increase in the centroid shift with ∼0.1 mm/s, due to the second-order Doppler shift); no magnetic coupling or major phase transition thus occurs at low temperature.

In the Raman spectrum (Fig. 11), a set of multiple bands in the region 860–1050 cm^{-1} are related to symmetric and antisymmetric stretching modes of Si–O bonds, whereas one at 680 cm^{-1} corresponds to the bending of Si–O–Si bridges. A distinct peak at 522 cm^{-1} is tentatively assigned to vibrations in the FeO_6 octahedra, whereas tetrahedrally coordinated Fe^{3+} is recognisable by a band around 630 cm^{-1}. The strongest band, in the low-wavenumber region at 185 cm^{-1}, is possibly related to Cl–Pb–Cl bending modes (Frost and Williams, 2004). The Raman spectrum is featureless from 1200 to 4000 cm^{-1}, and thus no signals were detected in the OH-vibration region, indicating an essentially anhydrous composition of jagoite.

Table 7. Mössbauer data for jagoite relative α-Fe

Centroid shift (mm/s)	Quadrupole splitting (mm/s)	Absorption area (%)	Assignment
298 K			
0.42(2)	0.50(2)	45(4)	$^{[6]}Fe^{3+}$
0.25(1)	1.22(2)	36(3)	$^{[4]}Fe^{3+}$
0.25(2)	0.45(3)	19(4)	$^{[4]}Fe^{3+}$
77 K			
0.51(4)	0.52(4)	43(8)	$^{[6]}Fe^{3+}$
0.34(2)	1.24(5)	38(7)	$^{[4]}Fe^{3+}$
0.34(3)	0.41(8)	19(4)	$^{[4]}Fe^{3+}$

Notes: Errors given as 2σ.

Discussion

Paragenesis

From textural relations, the main mineral components of the skarn (melanotekite, barysilite, andradite, hematite, quartz and diopside) can be inferred to be primary (associated with peak metamorphism). At some point, chlorine has been mobilised in the system; Whether it was available already in the primary mineralisation (Magnusson, 1930) or has been added in a later episode of geological evolution in the Långban area (Jonsson, 2003) has not been settled. The formation of jagoite and nasonite occurred at the expense of the pre-existing Pb minerals (for symbols see list in Table 6). Jagoite may be obtained directly from melanotekite and quartz via:

$$\underset{Mtk}{11\ Pb_2Fe_2Si_2O_9} + 2\ SiO_2 + 6\ HCl(aq) \rightarrow \underset{Jg}{2\ Pb_{11}Fe_5Si_{12}O_{41}Cl_3} + 6\ Fe_2O_3 + 3\ H_2O$$

Jagoite is a unique mineral in the $PbO–Fe_2O_3–SiO_2–Cl_2$ system. Hematophanite, $Pb_4Fe_3O_8Cl$ (without silica), probably forms under similar *P–T* conditions as jagoite but in a silica-undersaturated Pb–Fe-rich system (Holtstam *et al.*, 1995).

There is no sharp boundary between the metamorphic assemblage and the later recrystallisation products, as euhedral, poikiloblastic andradite may contain jagoite inclusions (Fig. 3a). This garnet growth could possibly be connected to a second temperature climax at Långban as inferred by Magnusson (1930). Grew *et al.* (1994) also reported a second generation of andradite in Pb-bearing Mn-skarn from Långban.

Some barysilite has been converted to alamosite by the reaction:

$$\underset{Bsl}{Pb_8Mn[Si_2O_7]_3} + 4\ SiO_2 + H_2O \rightarrow 7\ \underset{Aam}{PbSiO_3} + \underset{Ygi}{PbMnSi_3O_8{\cdot}H_2O},$$

which is supported by the fact that alamosite is more common than yangite in these assemblages.

The margarosanite–alamosite mixture noted in some samples could have formed by breakdown of ganomalite–wayneburnhamite (ganomalite is considered an early-formed

https://doi.org/10.1180/mgm.2025.10108 Published online by Cambridge University Press

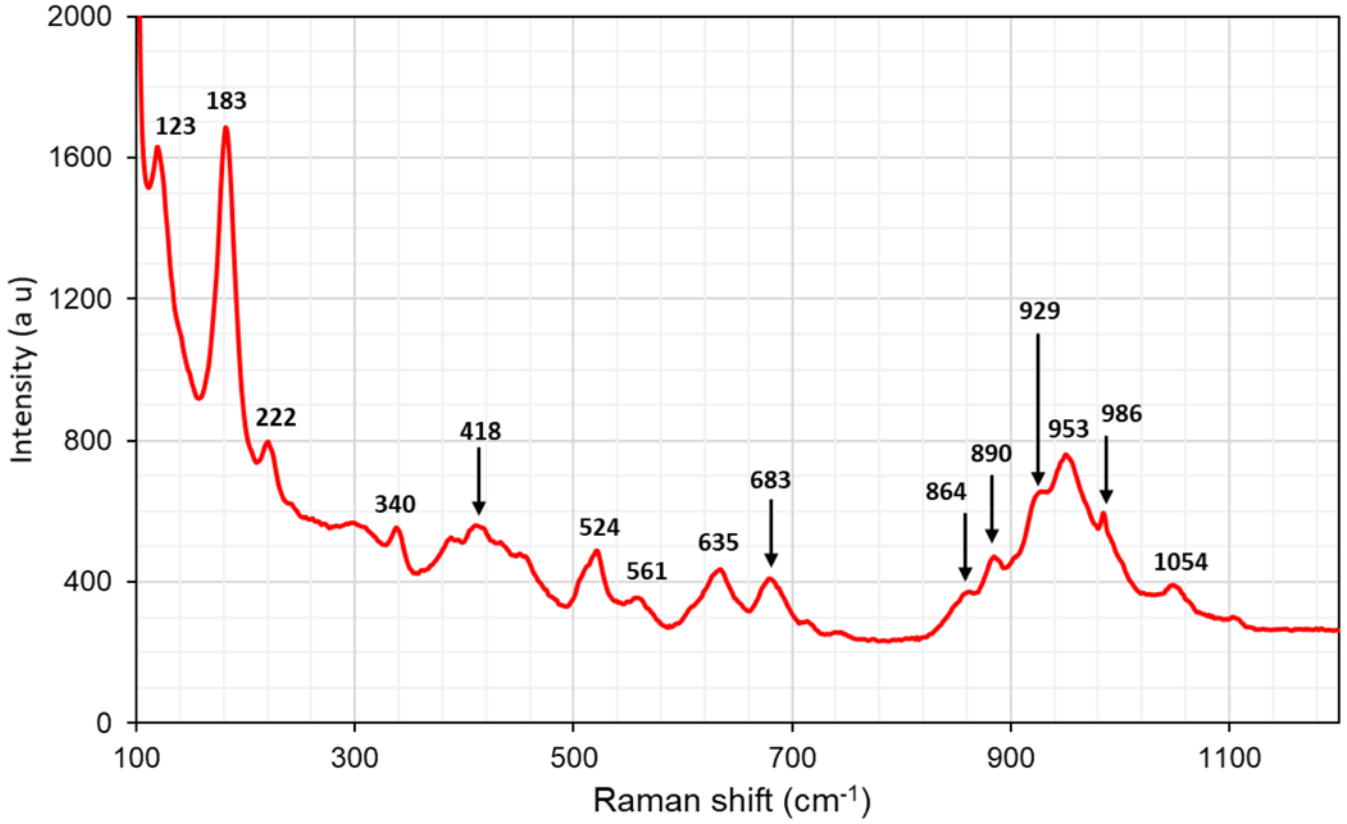


Figure 11. Raman spectrum of jagoite obtained with a 514 nm laser. Sample GEO-NRM #19410178.

skarn product in Långban; Magnusson, 1930) with the addition of silica:

$$\underset{Gnm}{Pb_9Ca_6Si_9O_{33}} + 6\ SiO_2 \rightarrow 3\ \underset{Mga}{PbCa_2Si_3O_9} + 6\ \underset{Aam}{PbSiO_3}$$

Hydrothermal alteration of the early lead silicates involving fluids bearing Ca^{2+} and SiO_2 (aq) has probably produced late-stage minerals. Our observations suggest alteration of jagoite to margarosanite according to a reaction like (Fig. 3a):

$$\underset{Jg}{Pb_{11}Fe_5Si_{12}O_{41}Cl_3} + 22\ Ca^{2+} + 21\ SiO_2 + 16\ H_2O \rightarrow 11\ \underset{Mga}{PbCa_2Si_3O_9} + 5\ Fe^{3+} + 3\ Cl^- + 32\ H^+$$

The unknown Pb–Ca–Cl–O–H silicate may have formed by a similar kind of reaction with the addition of Cl (see Fig. 3b):

$$2\ \underset{Jg}{Pb_{11}Fe_5Si_{12}O_{41}Cl_3} + 33\ Ca^{2+} + 16\ Cl^- + 31\ SiO_2\ (aq) + 43\ H_2O \rightarrow 11\ \underset{Ukn}{Pb_2Ca_3Si_5Cl_2(OH)_2{\cdot}2H_2O} + 10\ Fe^{3+} + 20\ H^+$$

The last two reactions are pH-dependent and rely on the fact that H^+ is consumed in the carbonate-rich environment. Calcium and SiO_2 have probably been released and made available for further reactions by the breakdown of diopside, forming serpentine or talc as additional products.

Hyttsjöite and the wickenburgite-like mineral may also be the result of hydrothermal alteration of jagoite (or the friisite mentioned). In the reactions suggested above, Pb is conserved in newly formed silicate minerals; the mechanisms of precipitation of native lead are not fully understood, (i.e. if it is related to breakdown of Pb silicate, or not).

During the transformation of the lead silicates, the molar ratio of metals (Pb, Ca, Mn, Fe and Al) to silicon in the products (Table 6) progressively diminish, with values ≤1 obtained for the latest alteration stage. Incorporation of structural H_2O is also a characteristic feature of some of the alteration products, indicating lower temperatures of crystallisation, probably <300°C, at this stage.

Crystal chemistry

Taking into account the refined site-scattering values (Table 4) and the polyhedron dimensions (Table 5), the best agreement between site-occupancy and average bond distances is found with the following crystal-chemical formula for jagoite:

$$^{[6]}Pb_2{}^{[7]}(Pb_{5.82}Ca_{0.18})_{\Sigma 6}{}^{[8]}(Pb_{2.88}Na_{0.12})_{\Sigma 3}{}^{[6]}[Fe^{3+}{}_{1.86}Al_{0.10}Sb^{5+}{}_{0.04}]_{\Sigma 2}[^{[4]}(Si_{3.80}Fe^{3+}{}_{1.02}Zn_{0.18})O_{14}][^{[4]}(Si_{8.78}Fe^{3+}{}_{0.54}Mn^{3+}{}_{0.48}Mg_{0.14}Be_{0.06})O_{27}](Cl_{2.86}Br_{0.02}O_{0.12})$$

Differences between observed site-scattering values and the ones calculated from the above crystal-chemical formula are reported in Table 8.

The assigned formula shows an 11% disagreement with the observed scattering at the *Si*2 site, which is rather high. However, the agreement is very good between observed and calculated mean bond distances, confirming the assignment of Mg to this site. The *Si*2 site is the largest among the fourfold coordinated sites and is the

https://doi.org/10.1180/mgm.2025.10108 Published online by Cambridge University Press

Table 8. Refined site-scattering values and assigned site-populations for jagoite (apfu = atoms per formula unit; epfu = electrons per formula unit)

Site*	Refined site-scattering (epfu)	Assigned site-population (apfu)	Calculated site-scattering (epfu)	$<X-\Phi>_{obs.}$** (Å)	$<X-\Phi>_{cal.}$*** (Å)	Ideal comp. (apfu)
$^{[6]}Pb1$	159.9	$Pb_{2.00}$	164.0	2.871	2.747	Pb_2
$^{[7]}Pb2$	467.4	$Pb_{5.82}Ca_{0.18}$	480.8	2.671	2.631	Pb_6
$^{[8]}Pb3$	224.1	$Pb_{2.82}Na_{0.12}$	237.5	2.819	2.817	Pb_3
Σ *Pb*	851.4	$Pb_{10.92}Ca_{0.18}Na_{0.08}$	882.3			Pb_{11}
$^{[6]}Fe$	51.4	$Fe^{3+}_{1.86}Al_{0.10}Sb^{5+}_{0.04}$	51.2	2.008	2.009	Fe^{3+}_2
*Si*1	52.5	$Si_{1.80}Fe^{3+}_{1.02}Zn_{0.18}$	52.4	1.710	1.730	Si_2Fe^{3+}
*Si*2	35.0	$Si_{0.82}Fe^{3+}_{0.54}Mn^{3+}_{0.48}Mg_{0.14}$	39.6	1.768	1.781	Fe^{3+}_2
*Si*3	28.0	$Si_{2.00}$	28.0	1.633	1.625	Si_2
*Si*4	26.3	$Si_{1.94}Be_{0.06}$	27.4	1.610	1.625	Si_2
*Si*5	84.0	$Si_{6.00}$	84.0	1.626	1.625	Si_6

*Coordination numbers are given for non-[4]-coordinated sites; **Φ = O, Cl; ***Calculated using ionic radii taken from Hawthorne and Gagné (2024).

tetrahedron connecting the two layers of tetrahedra of the double layer. The distortion index is particularly low (0.0011, the lowest among all the tetrahedra in the structure; Table 5) and excludes the possibility of allotting Zn to this site, as this element prefers a more distorted four-fold coordinated environment (for example, in willemite, Klaska *et al.*, 1978). In addition, assigning Zn to this site would increase the disagreement between observed and refined site-scattering values. Conversely, the *Si*1 site shows the highest distortion parameter among tetrahedra (0.0159; Table 5) and it is the other tetrahedron hosting Fe^{3+}. This site is also better suited to host Zn. Then the disagreement with observed site-scattering is very low (<1%), and the agreement is rather good between observed and calculated bond lengths, confirming the assignment of Zn and Fe^{3+} to this site. The higher polyhedron distortion is also in accord with the sharing of the bridging O4 anion site. This site is four-fold coordinated with one short and one long bond to the *Pb*2 site and two Si at the *Si*1 (Si_2Fe^{3+}) and *Si*3 (pure Si) sites, with a nominal charge incidence of $2 \times 2/8+0.917+1 = 2.417+$. Yet the bond-valence value at this site is acceptable (1.98 valence units, vu, Table 4) because the Pb–O bonds are rather long and the individual Si–O4 bond distance is the longest for these tetrahedra (Table 5). Such a relaxation mechanism of the structure imposes a strong deformation of the Si1 tetrahedron. The occurrence of a divalent cation at this site (Zn) also helps to match the bond-valence incidence at the O4 site. The *Si*4 sites probably host some Be (from LA-ICP-MS analyses, Table 2), but this does not account for its small size (it shows the smallest volume among all tetrahedra; Table 5). The lower volume among tetrahedra is related to the short Si–O7 bond, owing to the short O7–O7 distance along [0001], which is 2.74 Å, the edge shared by three Pb3 eight-fold polyhedra and the shortest among all the Pb3 polyhedron edges.

Another issue is the oxidation state of Mn and its partitioning among the sites. The best match between observed bond lengths and site scattering is obtained when considering all Mn as Mn^{3+}, ordered at the Si2 sites, because it has a shorter ionic radius than Mn^{2+} ($^{[4]}Mn^{3+}$–O = 1.901 vs. $^{[4]}Mn^{2+}$–O = 2.046 Å, Hawthorne and Gagné, 2024). The site is still dominantly occupied by trivalent atoms, but the Fe^{3+} is almost half of the amount present at the *Si*1 site. This is in better agreement with Mössbauer data, showing an ~2:1 relation between the two tetrahedrally coordinated Fe^{3+} sites. The absence of a perfect agreement is probably related to the fact that the weakest absorption doublet is not well resolved (Fig. 10). We believe that this is the best match between structural data and the Mössbauer spectrum and therefore a reasonable site assignment.

Charge balance requires some $Cl_{-1}O$ exchange at the *Cl* site. This replacement has been considered when calculating the bond-valence sums (BVS) reported in Table 5. In addition, the *Pb*1 site is six-fold coordinated with three at the O5 site and three Cl at the *Cl*1 site. A substitution allowing for vacancy, thus with less Cl at the *Cl* site, would further lower the bond valance incident at the *Pb*1 site. The introduction of some oxygen or bromine at this site helps to compensate for changes and bond valence incidence (as Br has a larger ionic radius than Cl). Overall, the calculated BVS are very good with only two oxygen sites slightly overbonded (BVS ~2.15 vu) which is still acceptable.

The polyhedron dimensions and site scattering suggest that Al-for-Fe^{3+} substitution occurs mainly at the Fe octahedra whereas Mn is ordered as Mn^{3+} at the less distorted *Si*2 tetrahedra. Antimony is probably pentavalent, occupying the Fe octahedra only. Coupled substitutions are inferred to incorporate divalent ions (Mg, Zn) in the jagoite structure, with excess Si^{4+} (above 12 atoms per formula unit): $2\ Fe^{3+} = Si^{4+} + M^{2+}$. From the large volume of the $Si2O_4$ tetrahedra (Table 5), it is inferred that trivalent species are mostly enriched there. The *Si*3 and *Si*5 sites are essentially filled with Si.

To define the ideal formula, we must consider charge balance and charge arrangements. On the one hand, the structure has 44 anion sites with a formal charge of –85 (41 O^{2-} + 3 Cl^-). On the other hand, the cation count of the structure is 28. Most of the site compositions correspond to almost fixed charges. The structure has 11 sites hosted by divalent Pb and 2 sites hosted by trivalent cations (Fe^{3+}) with six-fold coordination. These 13 cations sites account for 28+ charges. The other 15 cation sites left are in tetrahedral coordination. If we assume that all are occupied by Si^{4+} they would count for 60+ charges, with an excess of 3+ charges relative to the anion part. Some of the Si positions need to have less than 4+ average charges, and that can be achieved by substituting 3 Si^{4+} with 3 trivalent cations (in this case, Fe^{3+}). That leads us to the following charge arrangement for the ideal formula:

$$^{Pb1}(2+)_2\,^{Pb2}(2+)_6\,^{Pb3}(2+)_3\,^{M}(3+)_2\,^{T}[(4+)_{12}(3+)_3]^{O}(2-)_{41}\,^{Cl}(1-)_3$$

There are only significant heterovalent substitutions at two tetrahedral sites, *Si*1 (symmetry 6*g*) and *Si*2 (symmetry 4*e*), that

https://doi.org/10.1180/mgm.2025.10108 Published online by Cambridge University Press

account for 5 out of 15 sites with tetrahedral coordination. We could simply allocate all 3 Fe^{3+} at the *Si*1 site as it corresponds to 3 atoms pfu, thus obtaining a charge-balanced ideal formula. But it will be against structural evidence (observed mean bond length, polyhedral volume and site scattering; see Table 5 and Table 4, respectively) and local bond-valence requirements (in terms of bond valence; see Table 4). If we choose to substitute Si^{4+} by Fe^{3+} at the *Si*2 sites (2 apfu), it is not sufficient, and a further Fe^{3+} should be placed at the *Si*1 site. To make a choice, we should follow the dominant-valency and dominant-constituent rules in agreement with the definition of an ideal formula proposed by Hawthorne (2002), which implies that we may have mixed occupancy (and valence) at one site only. We could think of a situation with mixed occupancy at both *Si*1 ($SiFe^{3+}{}_2$) and *Si*2 ($SiFe^{3+}$), but it would be against the current definition of an ideal formula. The fact is that we need to have a mixed charge site for charge balance requirements, either *Si*1 or *Si*2. From a formal charge point of view, it does not make any difference. But from a local charge-balance (bond-valence) and symmetry constraints, it does. The choice of $^{Si2}Fe^{3+}$ and $^{Si1}(Si_2Fe^{3+})$ seems the best suited. Let us analyse the situation from the point of view of assigned site populations, symmetry restraints and local bond-valence requirements.

The double layer in the jagoite structure has 10 *T* sites (2 *Si*2, 2 *Si*4 and 6 *Si*5). In that layer, only 2 *T* sites (Si2) out of 10 are occupied by large cations (Fe^{3+}, Mn^{3+} and Mg) along with Si (see Table 8), which are those connecting the two layers. The heterogeneous composition (both in element and in charge) is reflected by the atomic displacement parameters (adp) of all the oxygen atoms bonded to the *Si*2 site, i.e. O6 and O9, which have the highest adp values among all the oxygen sites (Table 4). From data reported in Table 8, the dominant valence at the *Si*2 site is 3+ ($0.54\ Fe^{3+} + 0.48\ Mn^{3+} = 1.02 > 0.82\ Si^{4+} \gg 0.14\ Mg^{2+}$), and thus the dominant species of the dominant charge is Fe^{3+} ($Fe^{3+} > Mn^{3+}$). Therefore, in the ideal formula, we should write 2 Fe^{3+} apfu. That makes the ideal composition of the double layer to $[Fe^{3+}{}_2Si_8O_{27}]$. In the single layer, one site (*Si*3) is completely occupied by Si, whereas the other one (*Si*1) is occupied by 2 Si and one Fe^{3+} (plus 0.18 apfu of Zn), making the layer composition to $[Si_4Fe^{3+}O_{14}]$. With this choice, we obtain 3 Fe^{3+} at the tetrahedral sites in the ideal formula, thus fulfilling the charge arrangement required.

One could argue that we have not applied the dominant-valency rule for the *Si*1 site as we did for the *Si*2 site. But that would lead to 2 Fe^{3+} at the tetrahedral sites, imposing an excess of charge of 1+ in the charge balance of the ideal formula. Both *Si*1 and *Si*2 sites are in special positions: the *Si*1 site is at 6*e* and can only shift along [1000], the *Si*2 site is at 6*g* and can only shift along [1000]. However, the oxygen atoms coordinating these sites have different degrees of freedom. Both O2 and O4 atoms (coordinating *Si*1) occupy general positions, whereas among the ones coordinating the *Si*2 site, O6 is in a general position, but O9 is in a special position, 2*b*. In addition, O9 gets bond a valence-contribution also from the *Pb*3 sites that are in one special position (6*h*), whereas O2 and O4 sites get bond valence contribution from *Pb*2 sites, which occupy a general position (12*i*). The *Pb*2–O2 distance is the shortest in the *Pb*2 polyhedron, and this notably increases the bond valence incidence from Pb at the *Pb*2 site on the O2 site (0.44 vu calculated from the refined structural model). This compensates the required balance at O2, allowing it to achieve 1.96 vu (Table 4). This dictates the way that the structure can adapt locally to the chemical strain introduced by the $Si_{-1}Fe^{3+}$ heterovalent substitution. We have obtained excellent diffraction data and a very accurate determination of geometry that allowed us to produce a site assignment in agreement with observed site scattering and bond geometry (Table 8). These results show that the largest tetrahedral polyhedron is *Si*2, thus supporting our choice of full Fe^{3+} occupancy in the ideal formula. We cannot exclude a different site population for *Si*1 having more Fe^{3+} occupancy, but that must be balanced by the substitution of the trivalent Fe^{3+} by a small divalent cation at the *M* sites, like Mg. The introduction of Sb^{5+} at this site operates in the opposite way.

Mellini and Merlino (1981) suggested a scheme of ordering among cations (Si, Fe, Mn, Mg etc.) in the crystal structure that could lead to a different space-group symmetry; such a pattern was not confirmed with our data. We also solved the structure in space groups *P*31*c* and *P*321, obtaining models with the same topology and with split sites that are equivalent, i.e. no cation ordering was observed from refined site-scattering values nor observed sizes of polyhedra. Therefore, a reduction in space group symmetry was not justified.

Thus, taking into account all the above considerations, a structural charge-balanced formula for jagoite with coordination numbers indicated by superscripts would ideally be $^{[3+3]}Pb_2{}^{[7]}Pb_6{}^{[8]}Pb_3{}^{[6]}Fe_2\{^{[4]}[Si_2Fe^{3+}]^{[4]}[Si_2]\}_{single}\{^{[4]}[Fe^{3+}{}_2]^{[4]}[Si_2]^{[4]}[Si_6]\}_{double}O_{41}Cl_3$ (curly brackets enclosing the two layers of tetrahedra, single and double refer to layer widths of the tetrahedral layers), simplified to $Pb_{11}Fe_5Si_{12}O_{41}Cl_3$ for $Z = 2$.

Conclusions

Jagoite belongs to a far more diverse mineral association than suggested by the original description (Blix *et al.*, 1957). Primary lead silicates formed in the skarn during regional metamorphism, mainly melanotekite and barysilite, are susceptible to alteration, with Cl^-, SiO_2, Ca^{2+} and H_2O as the principal modifying agents. In the process, the relative Si contents of the products increase and reflect a higher degree of polymerisation of the SiO_4 units, along with hydration at lower temperatures under alkaline conditions. We conclude that most of the Pb is retained in silicate minerals during alteration overall; however, the mechanism of formation of sporadic occurrences of native Pb in some samples remains enigmatic.

The structural topology of jagoite, as described by Mellini and Merlino (1981), is confirmed with considerably improved data for the structural parameters. We have shown that minor elements are also hosted by jagoite, in particular Al at the octahedrally coordinated Fe site and Mn^{3+}, Zn and Mg at four-coordinated mixed Fe–Si sites. Jagoite crystals are also enriched in Be, Sb, Bi and Br, but these elements play a minor crystal-chemical role.

Supplementary material. The supplementary material for this article can be found at https://doi.org/10.1180/mgm.2025.10108.

Acknowledgements. The authors express their delight at the opportunity to contribute to this volume of the *Mineralogical Magazine* in honour of the eminent scientist Ed Grew, who has shown a long-standing interest in exotic mineral deposits, including Långban. We are most thankful to Guest Associate Editor Robert F. Martin and Sergey Krivovichev, Aaron Lussier and one anonymous journal referee for valuable reviews and recommendations.

Financial statement. F.C. acknowledges financial support from the Italian Ministry of Education (MUR) through the project "Dipartimenti di Eccellenza 2023–2027".

Competing interests. The authors declare none.

References

Baur W.H. (1974) The geometry of polyhedral distortions. Predictive relationships for the phosphate group. *Acta Crystallographica*, **3**, 1195–1215.

Blix R., Gabrielson O. and Wickman F.E. (1957) Jagoite, a new lead silicate mineral from Långban in Sweden. *Arkiv för mineralogi och geologi*, **2**, 315–317.

Boström K., Rydell H. and Joensuu O. (1979) Långban - An exhalative sedimentary deposit? *Economic Geology*, **74**, 1002–1011.

Brese N.E. and O'Keeffe M. (1991) Bond-valence parameters for solids. *Acta Crystallographica*, **B47**, 192–197.

Broz M.E., Cook R.F. and Whitney D.L. (2006) Microhardness, toughness, and modulus of Mohs scale minerals. *American Mineralogist*, **91**, 135–142.

Caulfield J.T., Tomlinson E.L., Chew DM., Marks M.A., McKenna C.A., Ubide T. and Smith V.C. (2020) Microanalysis of Cl, Br and I in apatite, scapolite and silicate glass by LA-ICP-MS. *Chemical Geology*, **557**, 119854.

Christy A.G. and Gatedal K. (2005) Extremely Pb-rich rock-forming silicates including a beryllian scapolite and associated minerals in a skarn from Långban, Värmland, Sweden. *Mineralogical Magazine*, **69**, 995–1018.

Dai Y., Post J.E. and Appleman D.E. (1995) Crystal structure of minehillite: Twinning and structural relationships to reyerite. *American Mineralogist*, **80**, 173–178.

Davis A., Drexler J.W., Ruby M.V. and Nicholson A. (1993) Micromineralogy of mine wastes in relation to lead bioavailability, Butte, Montana. *Environmental Science & Technology*, **27**, 1415–1425.

Dolomanov O.V., Bourhis L.J., Gildea R.J Howard J.A.K. and Puschmann H. (2009) OLEX2: A complete structure solution, refinement and analysis program. *Journal of Applied Crystallography*, **42**, 339–341.

Downs R.T., Pinch W.W., Thompson R.M., Evans S.H. and Megaw L. (2016) Yangite, $PbMnSi_3O_8 \cdot H_2O$, a new mineral species with double wollastonite silicate chains, from the Kombat mine, Namibia. *American Mineralogist*, **101**, 2539–2543.

Dunn P.J. (1985) The lead silicates from Franklin, New Jersey: occurrence and composition. *Mineralogical Magazine*, **49**, 721–727.

Dunn P.J. (1991) Rare minerals of the Kombat mine. *Mineralogical Record*, **22**, 421–25.

Frost R.L. and Williams P.A. (2004) Raman spectroscopy of some basic chloride containing minerals of lead and copper. *Spectrochimica Acta*, **60**, 2071–2077.

Gagné O.C. and Hawthorne F.C. (2015) Comprehensive derivation of bond-valence parameters for ion pairs involving oxygen. *Acta Crystallographica*, **B71**, 562–578.

Grew E.S., Yates M.G., Belakovskiy D.I., Rouse R.C., Su S.C. and Marquez N. (1994) Hyalotekite from reedmergnerite-bearing peralkaline pegmatite, Dara-i-Pioz, Tajikistan and from Mn skarn, Långban, Värmland, Sweden: A new look at an old mineral. *Mineralogical Magazine*, **58**, 285–297.

Grew E.S., Peacor D.R., Rouse R.C., Yates M.G., Su S.C. and Marquez N. (1996) Hyttsjöite, a new, complex layered plumbosilicate with unique tetrahedral sheets from Långban, Sweden. *American Mineralogist*, **81**, 743–753.

Hålenius U., Bosi F. and Gatedal K. (2013) Crystal structure and chemistry of skarn-associated bismuthian vesuvianite. *American Mineralogist*, **98**, 566–573.

Hawthorne F.C. (2002) The use of end-member charge-arrangements in defining new mineral species and heterovalent substitutions in complex minerals. *The Canadian Mineralogist*, **40**, 699–710.

Hawthorne F.C. and Gagné O.C. (2024) New ion radii for oxides and oxysalts, fluorides, chlorides and nitrides. *Acta Crystallographica*, **B80**, 326–339.

Hawthorne F.C., Uvarova Y.A. and Sokolova E. (2019) A structure hierarchy for silicate minerals: sheet silicates. *Mineralogical Magazine*, **83**, 3–55.

Hesse K.F., Liebau F. and Eulert H.H. (2003) Wickenburgite, a double-layer silicate $Pb_3Al^{[6]}[Ca^{[6]}Al^{[4]}Si^{[4]}{}_{10}O_{27}(H_2O)_3] \cdot H_2O$: Crystal chemistry and thermal behaviour. *Zeitschrift für Kristallographie-Crystalline Materials*, **218**, 542–552.

Holtstam D. and Langhof J. (editors) (1999) *Långban: the Mines, their Minerals, Geology and Explorers*. Raster Förlag, Stockholm. 215 pp.

Holtstam D. and Mansfeld J. (2001) Origin of a carbonate-hosted Fe-Mn-(Ba-As-Pb-Sb-W) deposit of Långban-type in Central Sweden. *Mineralium Deposita*, **36**, 641–657.

Holtstam D., Norrestam R. and Sjödin A. (1995) Plumboferrite: New mineralogical data and atomic arrangement. *American Mineralogist*, **80**, 1065–1072.

Holtstam D., Cámara F., Skogby H., Karlsson A. and Langhof J. (2019) Description and recognition of potassic-richterite, an amphibole supergroup mineral from the Pajsberg ore field, Värmland, Sweden. *Mineralogy and Petrology*, **113**, 7–16.

Holtstam D., Cámara F. and Karlsson A. (2024) Friisite, IMA 2024-047, in: CNMNC Newsletter 82. *European Journal of Mineralogy*, **36**, 1005–1010.

Jambor J.L. and Vaughan D.J. (editors) (1990) *Advanced Microscopic Studies of Ore Minerals*. Mineralogical Association of Canada Special Publication, 426 pp.

Jonsson E. (2003) Mineralogy and parageneses of Pb oxychlorides in Långban-type deposits, Bergslagen, Sweden. *GFF*, **125**, 87–98.

Jonsson E. and Broman C. (2002) Fluid inclusions in late-stage Pb–Mn–As–Sb mineral assemblages in the Långban deposit, Bergslagen, Sweden. *The Canadian Mineralogist*, **40**, 47–65.

Klaska K.-H., Eck J.C. and Pohl D. (1978) New investigation of willemite. *Acta Crystallographica*, **B34**, 3324–3325.

Lee D.E. (1958) An andradite-spessartite garnet from Pajsberg, Sweden. *American Mineralogist*, **43**, 208–215.

Li L., Zheng C., Fu Y., Wu D., Yang X. and Shen H. (2012) Silicate-mediated alleviation of Pb toxicity in banana grown in Pb-contaminated soil. *Biological trace element research*, **145**, 101–108.

Magnusson N.H. (1930) Långbans malmtrakt. *Sveriges Geologiska Undersökning*, **Ca 23**, 1–111.

Marks M.A., Kendrick M.A., Eby G.N., Zack T. and Wenzel T. (2017) The F, Cl, Br and I contents of reference glasses BHVO-2G, BIR-1G, BCR-2G, GSD-1G, GSE-1G, NIST SRM 610 and NIST SRM 612. *Geostandards and Geoanalytical Research*, **41**, 107–122.

Mellini M. and Merlino S. (1981) The crystal structure of jagoite. *American Mineralogist*, **66**, 852–858.

Merlino S. (1972) The crystal structure of zeophyllite. *Structural Science*, **28**, 2726–2732.

Merlino S. (1988) The structure of reyerite, $(Na, K)_2Ca_{14}Si_{22}Al_2O_{58}(OH).8.6 H_2O$. *Mineralogical Magazine*, **52**, 247–255.

Momma K. and Izumi F. (2011) VESTA 3 for three-dimensional visualization of crystal, volumetric and morphology data. *Journal of Applied Crystallography*, **44**, 1272–1276.

Moore P.B. (1970) Mineralogy & chemistry of Långban-type deposits in Bergslagen, Sweden. *The Mineralogical Record*, **1**, 154–172.

Prescher C., McCammon C. and Dubrovinsky L. (2012) MossA: a program for analyzing energy-domain Mössbauer spectra from conventional and synchrotron sources. *Journal of Applied Crystallography*, **45**, 329–331.

Sacerdoti M., Parodi G.C., Mottana A., Maras A. and Della Ventura G. (1993) Asbecasite: Crystal structure refinement and crystal chemistry. *Mineralogical Magazine*, **57**, 315–322.

Sheldrick G.M. (2015) SHELXT-integrated space-group and crystal-structure determination. *Acta Crystallographica*, **A71**, 3–8.

Siidra O.I., Zenko D.S. and Krivovichev S.V. (2014) Structural complexity of lead silicates: Crystal structure of $Pb_{21}[Si_7O_{22}]_2[Si_4O_{13}]$ and its comparison to hyttsjöite. *American Mineralogist*, **99**, 817–823.

Skelton A., Mansfeld J., Ahlin S., Lundqvist T., Linde J. and Nilsson J. (2018) A compilation of metamorphic pressure–temperature estimates from the Svecofennian province of eastern and central Sweden. *GFF*, **140**, 1–10.

Stephens M.B. and Jansson N. F. (2020) Paleoproterozoic (1.9–1.8 Ga) synorogenic magmatism, sedimentation and mineralization in the Bergslagen lithotectonic unit, Svecokarelian orogen. *The Geological Society, Memoir*, **50**, 155–206.

Warr L.N. (2021) IMA–CNMNC approved mineral symbols. *Mineralogical Magazine*, **85**, 291–320.

Williams S.A. (1968) Wickenburgite, a new mineral from Arizona, *American Mineralogist*, **53**, 1433–1438.

Zahoransky T., Friis H. and Marks M.A. (2016) Luminescence and tenebrescence of natural sodalites: a chemical and structural study. *Physics and Chemistry of Minerals*, **43**, 459–480.

https://doi.org/10.1180/mgm.2025.10108 Published online by Cambridge University Press